Supporting Information

Carbon Defects applied to potassium-ion batteries: A Density Functional Theory Investigation

Tongde Wang[a, #], Qian Li[a, #], Quantao Feng[a], Yidong Miao[a], Tianlin Li[a], Jiqiu Qi[a, *], Fuxiang Wei[a], Qingkun Meng[a], Yaojian Ren[a], Bin Xiao[a], Xiaolan Xue[a], Yanwei Sui[a, *], Zhi Sun[a, *]

[a] School of Materials and Physics, China University of Mining and Technology, Xuzhou 221116, People's Republic of China

*Corresponding authors. E-mails: flower_cumt@outlook.com (Jiqiu Qi); wyds123456@outlook.com (Yanwei Sui); 1455112915@qq.com (Zhi Sun)

# Tongde Wang and Qian Li contributed equally to this manuscript.

1. Computational Methods

In this paper, all calculations were conducted within density functional theory (DFT) using the Vienna Ab-initio Simulation Package (VASP, version 5.4.4).[1] The interactions between nuclei and valence electrons are described by a planewave basis set with the projector augmented wave (PAW) method,[2] and the electron exchange correlation potential is treated by the Perdew–Burke–Ernzerhof (PBE) functional under the Generalized Gradient Approximation (GGA).[3]

Lattice parameters and atomic positions were completely relaxed in the calculation, whose convergence tolerances of energy and ionic convergence criterion were set to 10^{-6} eV and 0.01 eV/Å. The energy cut-off for the plane waves was chosen to be 600 eV, to ensure the total energy was converged to 0.001 eV per atom. In view of the magnetic properties of some graphene doped systems, spin magnetization was turned on in the calculation. To correct for the effects of van der Waals (vdW) interactions, dispersion correction, known as DFT-D3, was used. Previous studies have shown that it has a good accuracy in the treatment of related adsorption systems.[4] All atomic charge distributions in our study were calculated by Bader Charge Analysis.[5]

The K-point is based on the gamma centered Monkhorst-Pack Grid method to generate Brillouin zone sampling. A 3*3*1 K-point space network is established for the structural optimization of the model, and a 6*6*1 K-point space network is established for the calculation of the corresponding density of states of the model. The single atom energy is calculated in the 20*20*20 Å cell to correct the adsorption energy

and improve the accuracy of calculation.

2. Experimental Section

2.1 Materials:

Sodium alginate (SA), urea, $NaNO_3$, acetylene black, PVDF, NMP, ethanol were ordered from Aladdin Reagents (Shanghai) Co., Ltd. All chemicals were used directly without any further treatment.

2.2 Synthesis of LPNCs:

The whole synthesis process includes gel preparation, liquid nitrogen freeze-drying, high-temperature carbonization, and water washing. First, 1 g SA was slowly added to 50 mL of deionized water in a water bath at 80 ℃ and stirred at a speed of 300 r/min for 2h to form a gelatinous solution similar to jelly. Then, 0.75 g urea and 0.75 g NaNO3 were added into the uniform sol and continued stirring for 30min to ensure the full dissolution of the molten salt. The sol was placed in liquid nitrogen for 3 min, and then the gel was freeze-dried in a vacuum freeze-dryer for 48 h (the freezing condition was - 45℃, the vacuum condition was 1 Pa) to get light aerogel. The carbonization process at high temperature refers to that the aerogel obtained above is heated at 800 ℃ for 1 hour in high purity nitrogen at a flow rate of 20 $cc \cdot min^{-1}$ and a heating rate of 3 $℃ \cdot min^{-1}$. Subsequently, the water-soluble inorganic on the black product was fully washed and filtered with deionized water. Finally, the precipitate was dried in a blast dryer at 60 ℃ for 24 h to obtain the final product LPNCs. LPCs was synthesized in the same way except without urea.

2.3 Characterization and Electrochemical Tests:

he crystal structure and phase composition were analyzed by X-ray diffraction (XRD, Bruker D8) with Cu Kα radiation (λ=0.1518nm). between 10 and 80°. X-ray photoelectron spectroscopy (XPS, Thermo ESCALAB 250XI) was used to determine the chemical state of samples.

Electrodes were prepared by mixing 85 wt% of active materials, 5 wt% of acetylene black, and 5 wt% of PVDF in dispersant (NMP). The uniformly ground slurry was coated with designated thickness onto copper (for anode), drying at 120 °C for 12 h under vacuum. Assembling K half-cells (CR2032) with K wafer as the counter electrode to test the properties of LPCs/LPNCs anode.

Cyclic voltammetry test and charge and discharge test were carried out at 0.01 ~ 3.0V voltage, tested by Land cell measurement system (Wuhan Land Electronics Co., Ltd.) at a current density of 10 A g^{-1}. The cyclic voltammetry (CV), galvanostatic charge/discharge (GCD) were carried out at CHI 660E electrochemical workstation (Shanghai ChenHua Instrument Co., Ltd.).

Table S1. Calculated geometric structure information

Defect	C-C(Å)	C-N(Å)	C-P(Å) / C-S(Å)	C-C-C (°)	C-N-C (°)	C-P-C (°) / C-S-C (°)
Non-defective	1.423	--	--	120	--	--
SV	1.368- 1.474	--	--	115-127	--	--
SW	1.307-1.463	--	--	99-142	--	--
Nc1	1.418	1.412	--	120	120	--
Nc2-1	1.411-1.518	1.329	--	110-126	122	--
Nc2-2	1.382-1.448	1.336-1.357	--	119-126	122	--
Nc2-3	1.420-1.453	1.339	--	119-121	122	--
Nc3	1.349-1.450	1.456	--	110-126	108	--
Pc1	1.401-1.423	--	1.762	120-122	--	100
Sc1	1.4-1.423	--	1.744	121-123	--	101

Table S2. Adsorption energy (in eV) on defective carbon surface.

Defect	H1	H2	H3	T1	B1
Non-defective	-1.134	--	--	-1.056	-1.061
SV	-2.247	-1.957	-1.903	-1.986	-2.065
SW	-1.561	-1.542	--	-1.521	-1.533
Nc1	-0.864	--	--	-0.784	-0.799
Nc2-1	-2.481	-2.461	-2.036	-2.443	-2.07
Nc2-2	-2.656	-1.961	-1.905	-2.176	-1.957
Nc2-3	-3.164	-2.089	-1.993	-2.452	-2.122
Nc3	-2.501	-2.145	-1.904	-2.307	-1.937
Pc1	-1.844	-1.587	-1.576	-1.979	-1.668
Sc1	-1.19	-1.001	-1.03	-1.221	-1.058

Table S3. Metal adsorption energy (in eV) on defective carbon surface.

Defect	K	Li	Na
Non-defective	-1.134	-1.242	-0.685
SV	-2.247	-2.696	-2.012
SW	-1.561	-2.062	-1.52
Nc1	-0.864	-0.822	-0.58
Nc2-1	-2.481	-3.051	-2.242
Nc2-2	-2.656	-3.694	-2.523
Nc2-3	-3.164	-4.695	-3.120
Nc3	-2.501	-3.421	-2.411
Pc1	-1.979	-2.072	-1.52
Sc1	-1.221	-1.253	-0.54

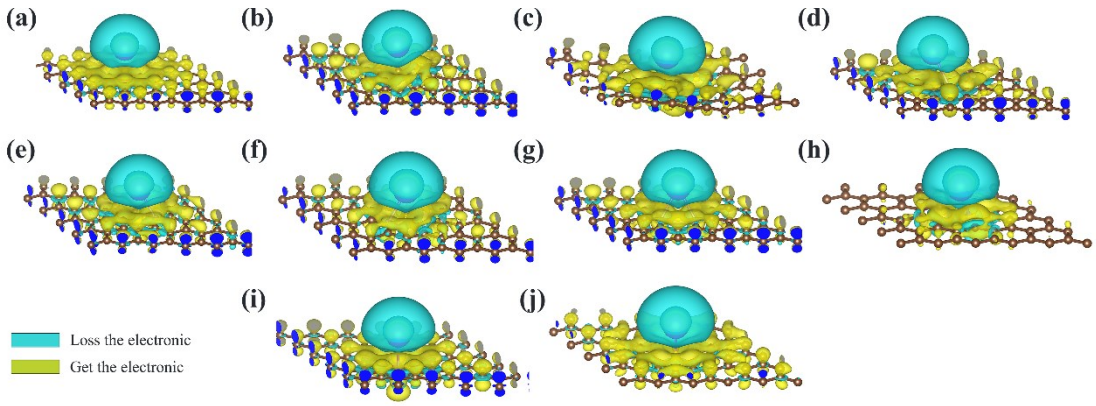

Figure S1. Charge density difference plots for K adsorption on (a) Intrinsic graphene (b) single vacancy (SV) (c) Stone-Wales defects (SW) (d) graphitic -N (Nc1) (e) a nitrogen substituted pyridinic-N (Nc2-1) (f) two nitrogen substituted pyridinic-N (Nc2-2) (g) three nitrogen substituted pyridinic-N (Nc2-3) (h) pyrrolic -N (Nc3) (i) Phosphorus-containing defect (Pc1) (j) Sulfur-containing defect (Sc1) Structures were visualized with VESTA. [6]

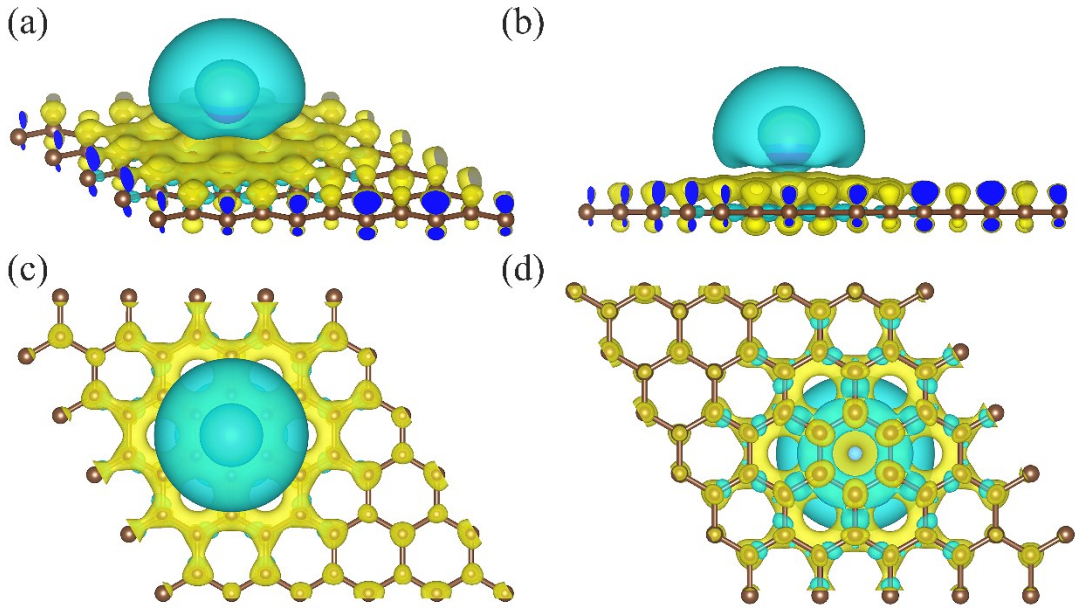

Figure S2. Charge density difference plots for K adsorption on Intrinsic graphene (a) The conventional (b) Front view (c) Vertical view (d) Bottom view

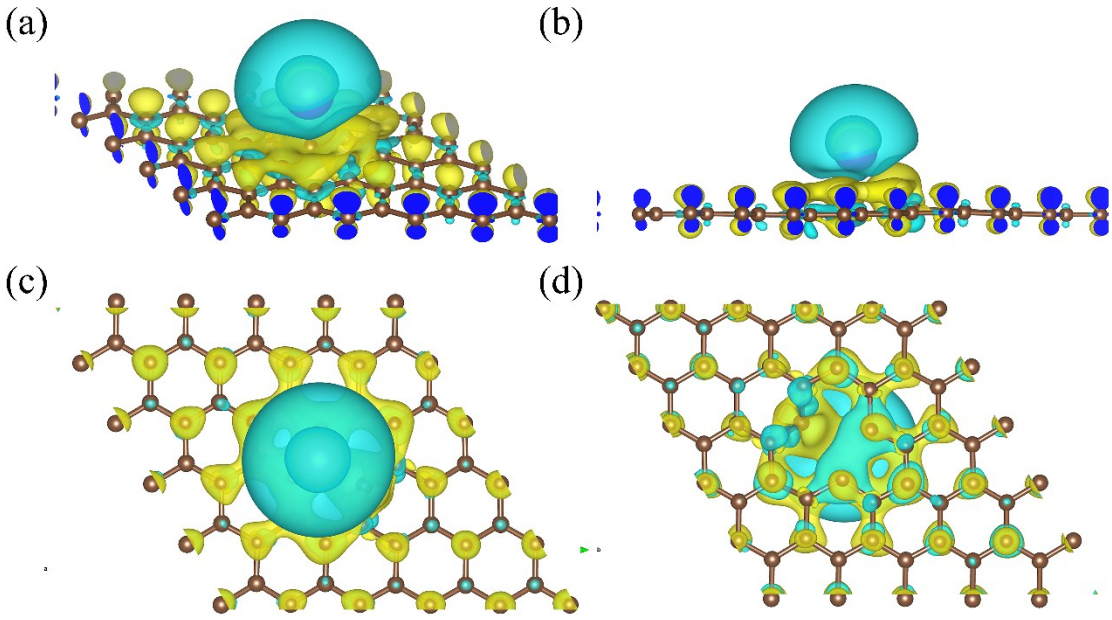

Figure S3. Charge density difference plots for K adsorption on single vacancy (SV) (a) The conventional (b) Front view (c) Vertical view (d) Bottom view

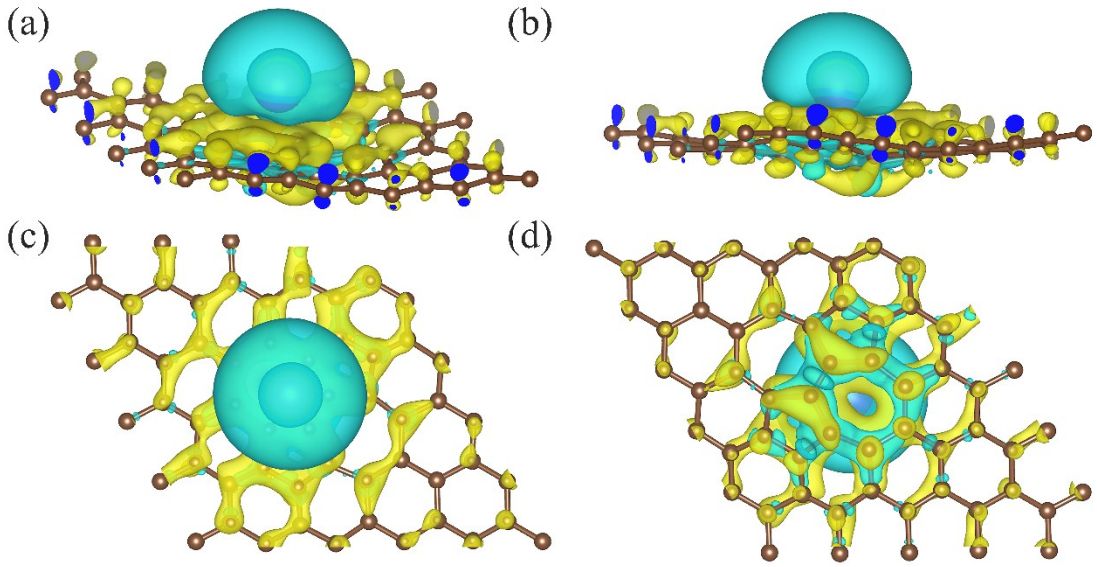

Figure S4. Charge density difference plots for K adsorption on Stone-Wales defects (SW) (a) The conventional (b) Front view (c) Vertical view (d) Bottom view

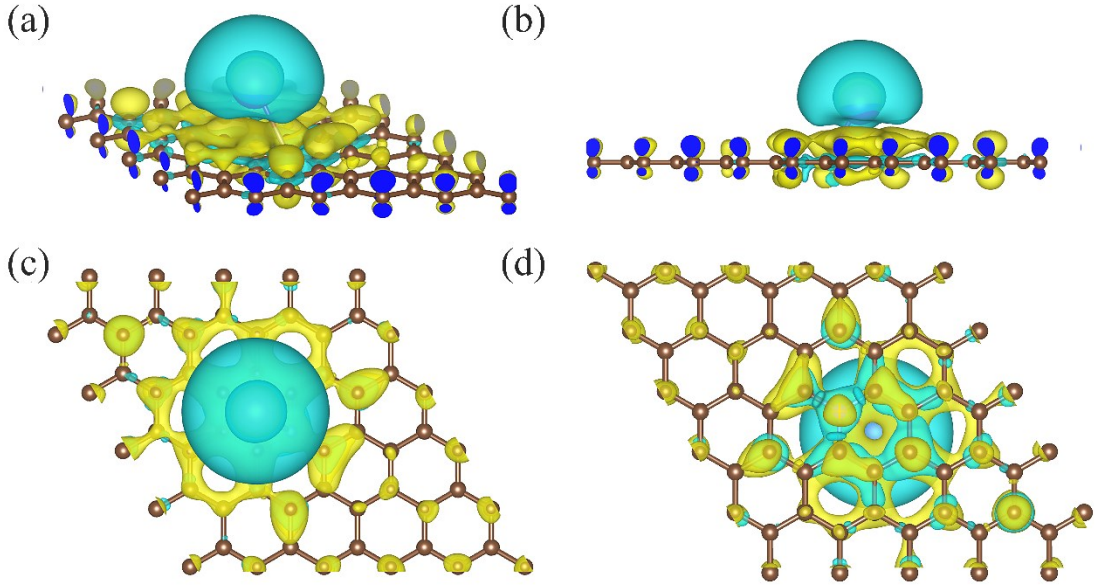

Figure S5. Charge density difference plots for K adsorption on graphitic -N (Nc1) (a) The conventional (b) Front view (c) Vertical view (d) Bottom view

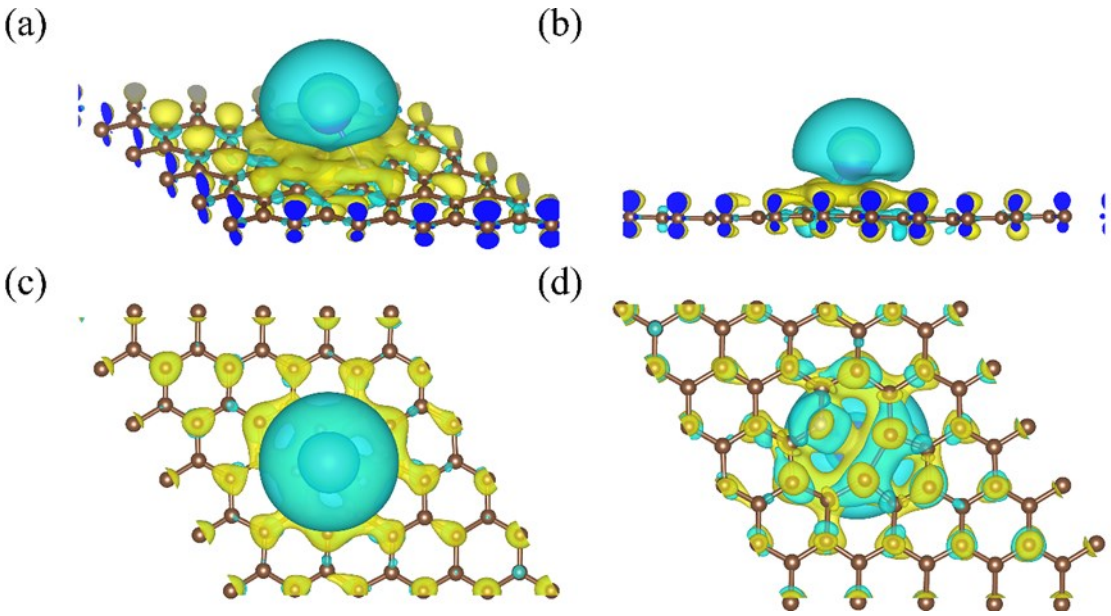

Figure S6. Charge density difference plots for K adsorption on a nitrogen substituted pyridinic-N (Nc1Vc1) (a) The conventional (b) Front view (c) Vertical view (d) Bottom view

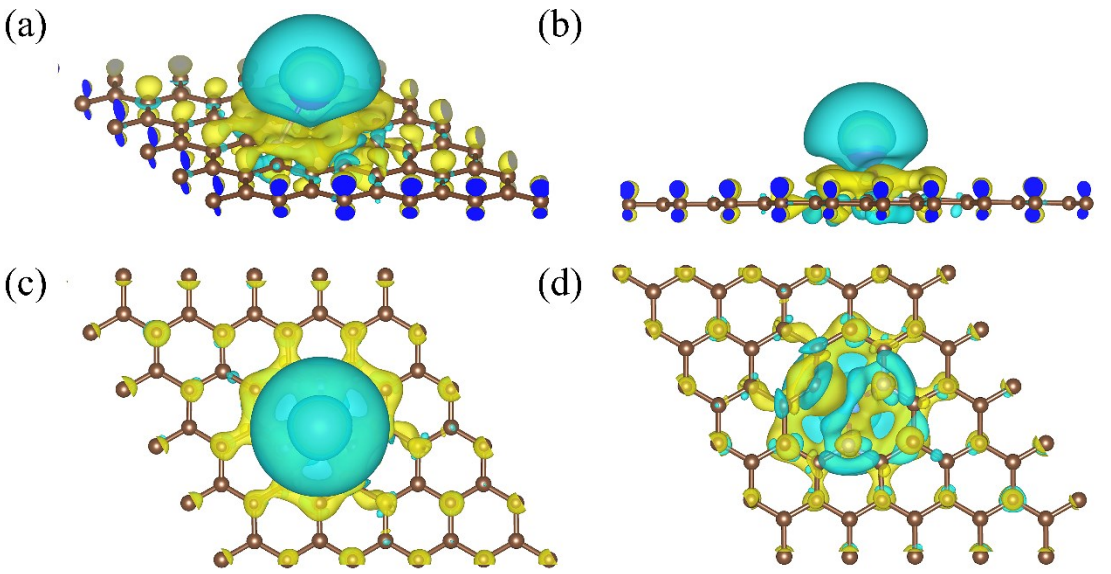

Figure S7. Charge density difference plots for K adsorption on two nitrogen substituted pyridinic-N (Nc2Vc1) (a) The conventional (b) Front view (c) Vertical view (d) Bottom view

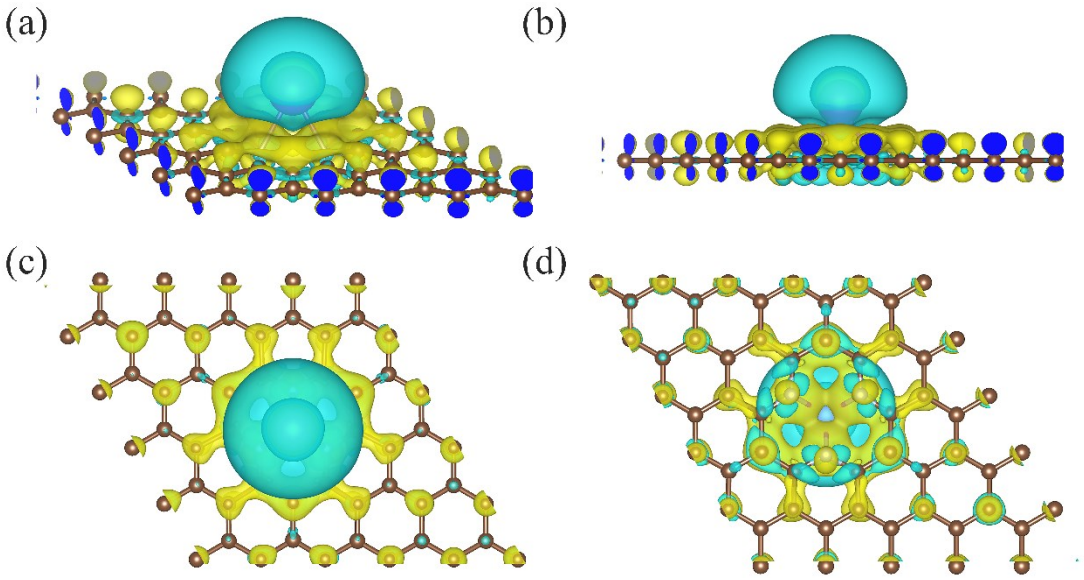

Figure S8. Charge density difference plots for K adsorption on three nitrogen substituted pyridinic-N (Nc3Vc1) (a) The conventional (b) Front view (c) Vertical view (d) Bottom view

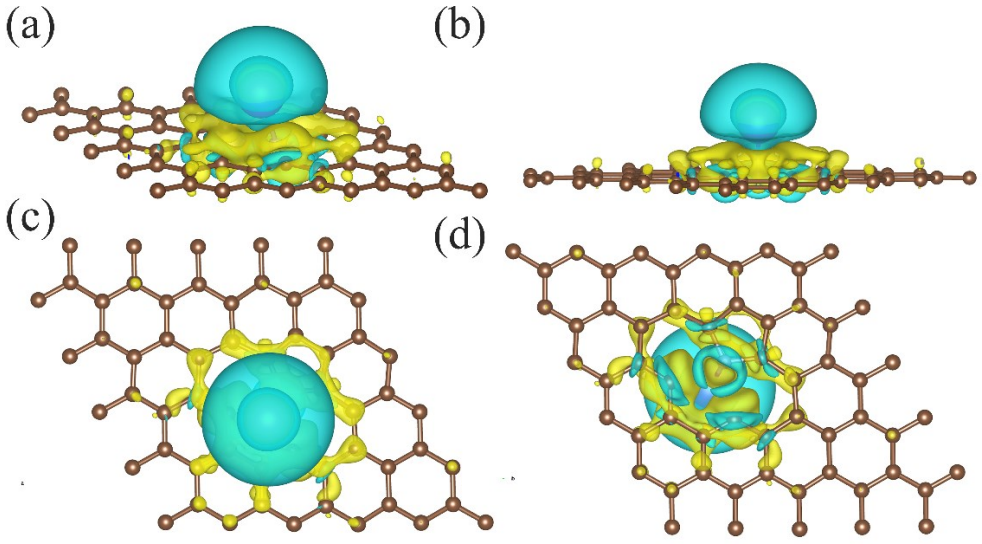

Figure S9. Charge density difference plots for K adsorption on three nitrogen substituted pyridinic-N (Nc3Vc1) (a) The conventional (b) Front view (c) Vertical view (d) Bottom view

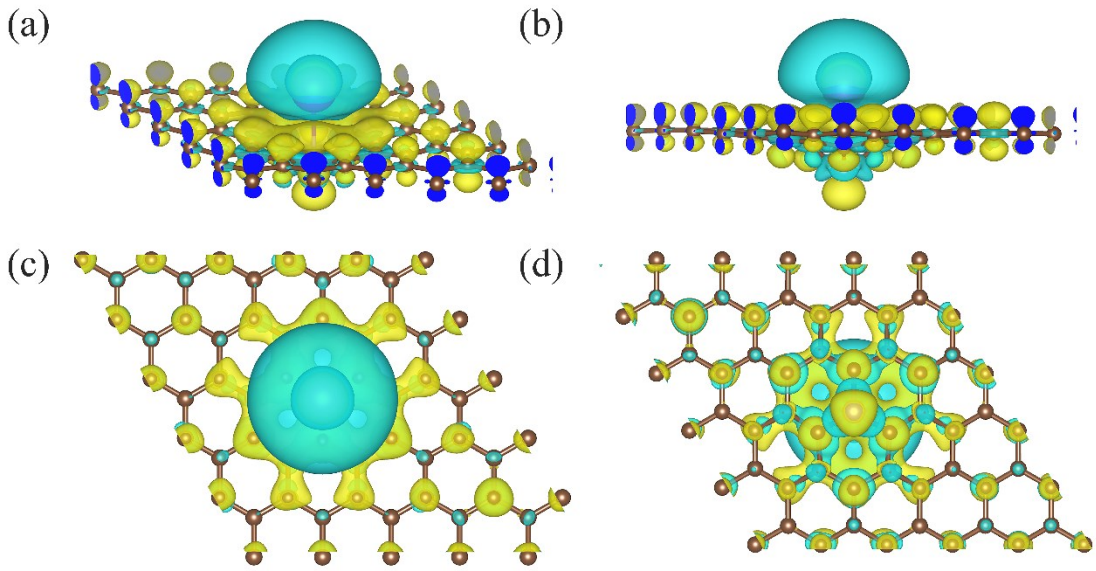

Figure S10. Charge density difference plots for K adsorption on Phosphorus-containing defect (Pc1) (a) The conventional (b) Front view (c) Vertical view (d) Bottom view

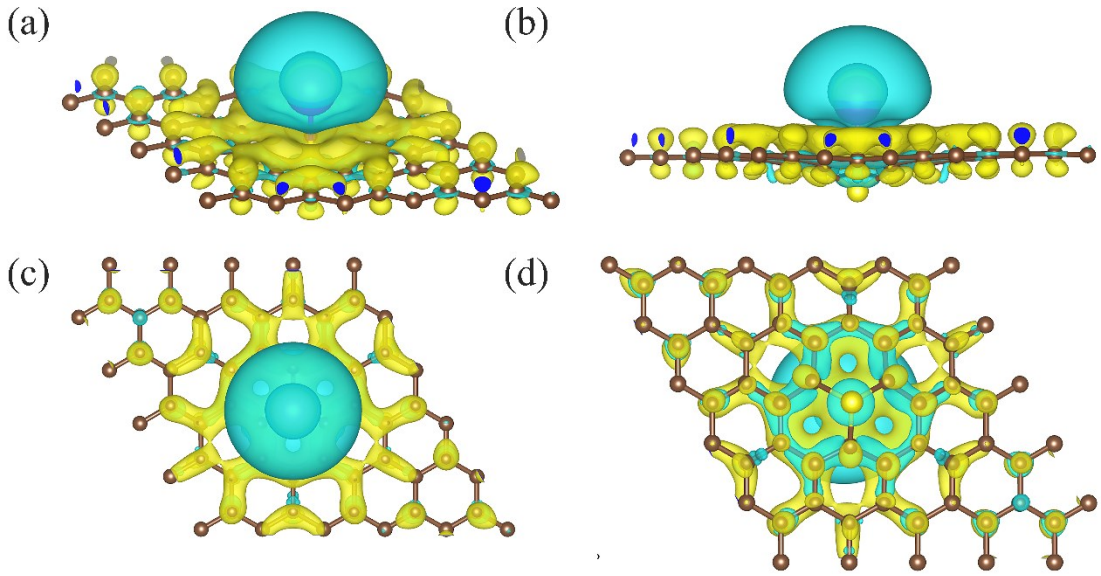

Figure S11. Charge density difference plots for K adsorption on Sulfur-containing defect (Sc1) (a) The conventional (b) Front view (c) Vertical view (d) Bottom view

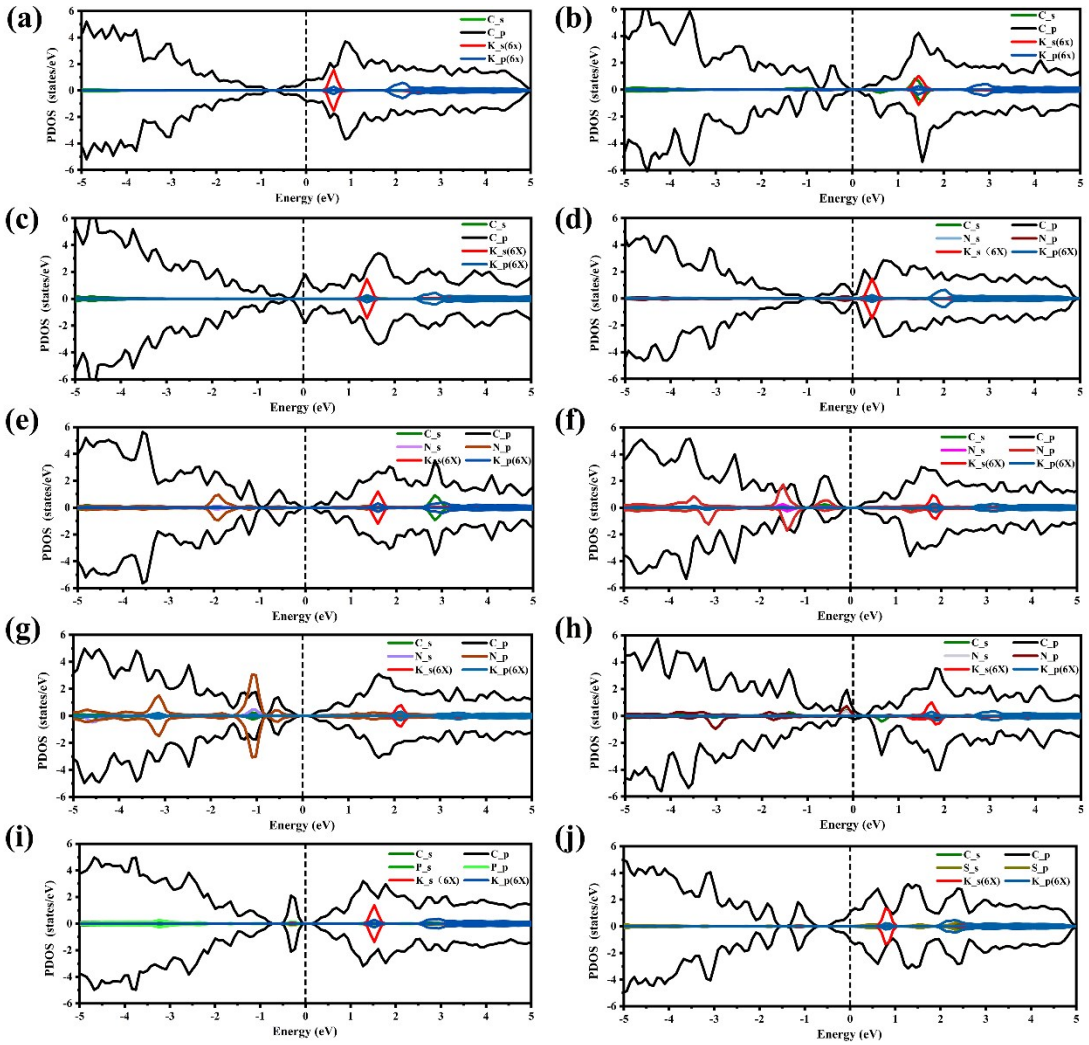

Figure S12. Density of states (after adsorption) of the (a) Intrinsic graphene (b) SV (c) SW (d) Nc1 (e) Nc2-1 (f) Nc2-2 (g) Nc2-3 (h) Nc3 (i) Pc1 (j) Sc1

Table S4. The occupied state (in eV) of K (after adsorption)

Defect	Energy
Non-defective	0.618
SV	1.449
SW	1.396
Nc1	0.424
Nc2-1	1.594
Nc2-2	1.809
Nc2-3	2.149
Nc3	1.726
Pc1	1.527
Sc1	0.782

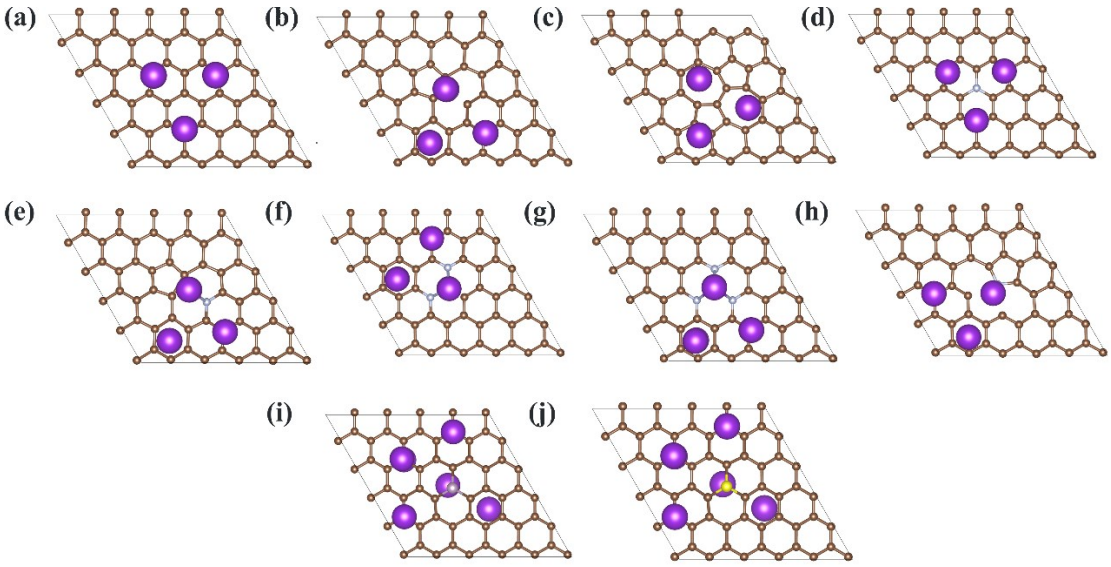

Figure S13. The optimized geometries of six K atoms adsorbed on (a) Intrinsic graphene (b) SV (c) SW (d) Nc1 (e) Nc2-1 (f) Nc2-2 (g) Nc2-3 (h) Nc3 (i) Pc1 (j) Sc1 (Some of the atoms are symmetrical based on the graphene plane)

Table S5. The relationship between the average adsorption energies (in eV) and the number of K on graphene structures.

Defect	1	2	3	4	5	6	8	11	14
Non-defective	-1.134	-1.032	-0.955	-0.923	-0.865	-0.771	--	--	--
SV	-2.247	-1.583	-1.361	-1.209	-1.176	-1.159	-0.99	-0.943	-0.902
SW	-1.561	-1.156	-1.054	-1.031	-1.001	-0.988	-0.913	--	--
Nc1	-0.864	-0.806	-0.762	-0.721	-0.686	-0.647	--	--	--
Nc2-1	-2.481	-1.682	-1.467	-1.365	-1.226	-1.162	-0.992	-0.939	-0.905
Nc2-2	-2.656	-1.878	-1.495	-1.352	-1.252	-1.186	-1.033	-0.967	-0.929
Nc2-3	-3.164	-1.985	-1.739	-1.626	-1.421	-1.347	-1.134	-1.015	-0.935
Nc3	-2.501	-1.705	-1.477	-1.369	-1.264	-1.169	-1.041	-1.013	-0.905
Pc1	-1.979	-1.331	-1.185	-0.998	-0.930	-0.871	--	--	--
Sc1	-1.221	-1.042	-0.876	-0.744	-0.701	-0.651	--	--	--

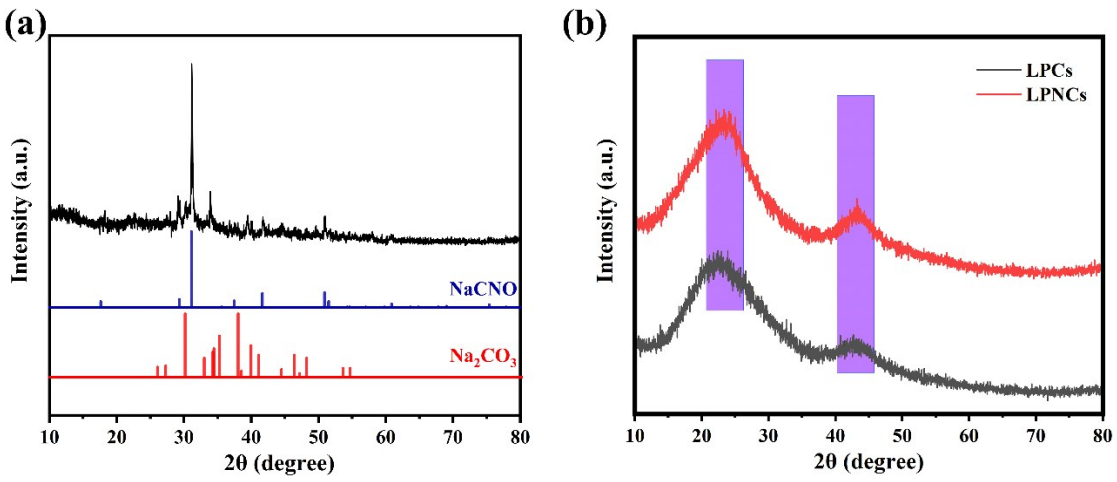

Figure S14. XRD patterns of (a) LPNCs before cleaning (b) LPCs/LPNCs after cleaning

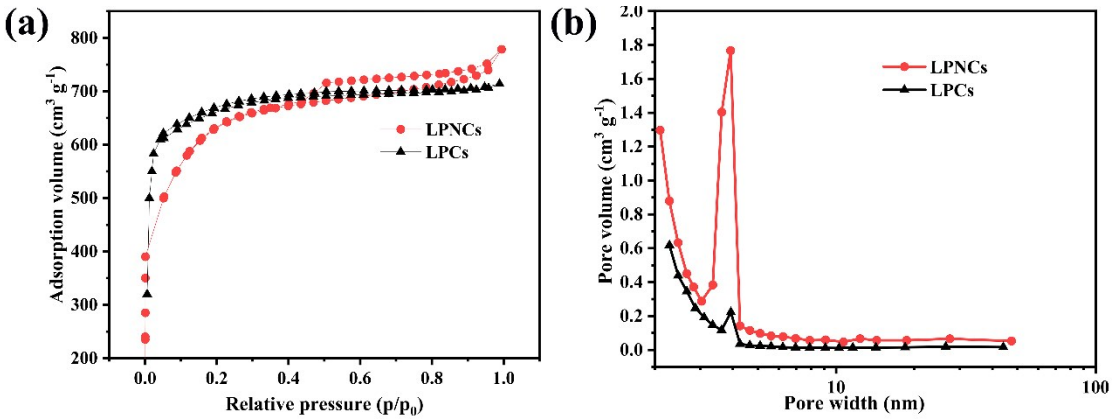

Figure S15. (a) N_2 adsorption/desorption isotherm of LPNCs/LPCs (b) pore size distribution curves of LPNCs/LPCs

Reference

1. Kresse, G.; Hafner, J., 14251; G. Kresse, J. Furthmüller. Phys. Rev. B 1996, 54, 11169.

2. Kresse, G.; Joubert, D., From Ultrasoft Pseudopotentials to the Projector Augmented-Wave Method. Physical review b 1999, 59, 1758.

3. Perdew, J. P.; Ernzerhof, M.; Burke, K., Rationale for Mixing Exact Exchange with Density Functional Approximations. The Journal of chemical physics 1996, 105, 9982-9985.

4. Grimme, S.; Antony, J.; Ehrlich, S.; Krieg, H., A Consistent and Accurate Ab Initio Parametrization of Density Functional Dispersion Correction (Dft-D) for the 94 Elements H-Pu. The Journal of chemical physics 2010, 132, 154104.

5. Tang, W.; Sanville, E.; Henkelman, G., A Grid-Based Bader Analysis Algorithm without Lattice Bias. Journal of Physics: Condensed Matter 2009, 21, 084204.

6. Momma, K.; Izumi, F. J. J. o. a. c., Vesta 3 for Three-Dimensional Visualization of Crystal, Volumetric and Morphology Data. 2011, 44, 1272-1276.